

Correlations among neutron-proton and neutron-deuteron elastic scattering observables

Yu. Volkotrub

*AGH University of Science and Technology,
Faculty of Physics and Applied Computer Science, PL-30055 Kraków, Poland*

R. Skibiński, J. Golak, and H. Witała

*M. Smoluchowski Institute of Physics,
Jagiellonian University, PL-30348 Kraków, Poland*

(Dated: May 31, 2022)

Abstract

We employ two models of the nucleon-nucleon force: the OPE-Gaussian as well as the chiral $N^4\text{LO}$ and $N^4\text{LO}^+$ interactions with semilocal regularization in momentum space to study correlations among two-nucleon and three-nucleon elastic scattering observables. These models contain a number of free parameters whose values and covariance matrices are evaluated from a fit to the two-nucleon data. Such detailed knowledge of parameters allows us to create, using various sets of statistically generated parameters, numerous versions of these potentials and next apply them to two- and three-nucleon scattering to make predictions of various observables at the reaction energies up to 200 MeV. This permits a systematic analysis of correlations among two-nucleon and three-nucleon observables, basing on a relatively big sample of predictions. We found that most observables in neutron-proton and neutron-deuteron systems are uncorrelated, but there are exceptions revealing strong correlations, which depend on the reaction energy and scattering angle. This information may be useful for precise fixing free parameters of two-nucleon and three-nucleon forces and for understanding dependencies and correlations between potential parameters and observables.

PACS numbers: 21.45.-v, 25.10.+s, 13.75.Cs

I. INTRODUCTION

One of the challenges in nuclear physics is to describe *ab initio*, i.e. starting from reliable models of the nucleon-nucleon (NN) and many-nucleon forces, properties of nuclear systems and reactions. The current understanding of the nuclear forces is that they are residual interactions of the strong forces between quarks and gluons. Nowadays we are not able to apply Quantum Chromodynamics (QCD) directly in the non-perturbative region and to describe processes at the nuclear scale starting from quarks and gluons and their interactions.

Instead various effective models of nuclear interactions have been prepared. The Argonne v18 (AV18) [1] and the CD-Bonn [2] models of NN interaction are important examples which provide a quite satisfactory description of numerous nuclear phenomena. The quality of two-nucleon (2N) data description can be measured by the χ^2/datum value obtained from a comparison of theoretical predictions and experimental data. The AV18 and CD-Bonn forces achieved χ^2/datum close to 1 but by using 40 and 45 free parameters, respectively. These parameters were fitted, via the phase shifts obtained by the Nijmegen group [3], to all 2N data available at that time. In both cases, only the central values of the parameters were determined and no information about their uncertainties, to the best of our knowledge, was published. A serious disadvantage of these models is the lack of a direct link to QCD. This issue does not occur in the models of nuclear forces derived within the χ EFT approach [4] such as the recent potential with the semi-local regularization in momentum space (SMS) proposed by the Bochum-Bonn group [5] or the forces derived by R. Machleidt *et al.* [6], M. Piarulli *et al.* [7] and others [8].

In the course of time, as the more and more advanced nuclear force models were derived, the accurate determination of their free parameters became more and more important. The crucial step was taken by R. Navarro Pérez and his collaborators from the Granada group. They revised the available 2N data and prepared a new database [9], rejecting experimental results for which the experimental uncertainties were unknown or poorly defined. They excluded also data sets inconsistent with other experimental results. This procedure led to consistency of the eventually accepted data sets. The Granada-2013 database is currently a standard collection of data used for fixing parameters of the NN forces.

For some models of the NN interaction, derived in the 21st century, like the OPE-Gaussian force [10] or the chiral SMS force [5], in addition to the central values of parameters also their covariance matrices were determined. This has opened up new possibilities in few-nucleon studies. The propagation of the uncertainties of the potential parameters from a 2N system to many-body observables is one example. We have studied this issue in [11, 12] and determined for the first time in a quantitative way the corresponding theoretical uncertainties for the elastic nucleon-deuteron (Nd) observables. Another interesting problem that can be investigated with the help of the covariance matrix of the potential parameters is the existence of correlations among various observables in two- and three-nucleon (3N) systems as well as between observables and specific potential parameters. In particular this can lead to establishing a set of observables that should (should not) be taken into account while fixing the free parameters of the three-nucleon force (3NF). The free parameters of the older 3NF models, like the Tucson-Melbourne [13–15] or the UrbanaIX [16] were determined from the ^3H binding energy and the density of the nuclear matter. In the case of the chiral models, for which the 3NF occurs for the first time at N^2LO [17, 18], its two free parameters (c_D and c_E) were initially fixed from the ^3H binding energy and the neutron-deuteron (nd) doublet scattering length $^2a_{nd}$ [17, 19]. However, it is known that these two observables are strongly

correlated and their linear dependence manifests itself in the so-called Phillips line [20]. More recently, in Ref. [21], beside the ${}^3\text{H}$ binding energy, the differential cross section at $E_{\text{lab}} = 70$ MeV around its minimum was used instead of ${}^2a_{\text{nd}}$ for a 3NF consistent with the SMS regularization. The choice of the cross section was dictated by the significant 3NF effects observed in this angular region and by the existence of the very precise experimental data [22]. In Ref. [23] authors discussed also the dependence of the c_D and c_E values on the choice of the energy and scattering angle ranges used during the fixing procedure, and found it small.

However, the question of possible correlation between the ${}^3\text{H}$ binding energy and the scattering cross section is still open. The answer is important since obviously using the strongly correlated observables to fix free parameters can bias the results of such a determination method. Moreover, thirteen new free parameters, namely strengths of contact terms, for 3NF are expected at N^4LO [24]. Fixing them will be a tremendous computational effort, and therefore the set of observables used for this purpose must be carefully selected. Specifically, to minimize uncertainties of fixed parameters, the selected observables should be uncorrelated. While the use of emulators proposed in [25, 26] can reduce the amount of required CPU time, the accuracy of parameter values will still depend on a set of input observables. Similarly, correlations discovered in the 2N system could impact the procedures used to fix free parameters of the NN force.

In the past a study of correlations was not possible at a statistically significant level, due to the lack of a sufficiently large number of the realistic models of the nuclear potential and precise data. The situation has changed in recent years. Using the OPE-Gaussian or the chiral SMS forces allows us to prepare many sets of the potential parameters and thus, after a procedure described in the next section, obtain a number of predictions large enough to analyze correlations and to draw quantitative conclusions. Some attempts to study correlations in few-nucleon sectors are presented in Refs. [27], [28] and [29]. In Ref. [27] the authors study, using the Monte-Carlo bootstrap analysis as a method to randomize proton-proton and neutron-proton (np) scattering predictions, correlations between the ground states of the ${}^2\text{H}$, ${}^3\text{H}$ and ${}^4\text{He}$ binding energies, focusing mainly on the Tjon line [30], i.e. the correlation between ${}^3\text{H}$ and ${}^4\text{He}$ binding energies, but do not investigate the scattering observables. In Ref. [28] the correlations between three- and four-nucleon observables have been investigated within the pionless Effective Field Theory with the Resonating Group Method. Because this approach can be applied only to processes at very low energies the authors focus on the study of bound-state properties and the ${}^3\text{H}$ -neutron S -wave scattering length, finding the latter correlated with the ${}^3\text{H}$ binding energy. Kievsky *et al.* [29] studied correlations among the low-energy bound state observables in the two- and three-nucleon systems, extending this research to some features of the light nuclei and beyond up to nuclear matter and neutron star properties. Using a simple model of “Leading-order Effective Field Theory inspired potential” they found evidence of the connection between few- and many-nucleon observables. In addition, in Ref. [31] correlations among partial wave dependent parameters in NN scattering, arising from the experimental data have been discussed in the context of uncertainty of models of the nuclear interaction. None of these works is focused on correlations in the context of three-nucleon observables.

In the present paper we study correlations among observables in neutron-proton elastic scattering as well as among observables in neutron-deuteron elastic scattering focusing on the latter ones. The paper is organized as follows: in Sec. II we list the essential steps of our formalism. In Secs. III and IV we show results on correlations among various two- and

three-nucleon observables, respectively. Finally, we summarize and conclude in Sec. V.

II. FORMALISM

The realization of our work can be split into the following phases:

- (1) Preparation of sets of the potential parameters

Having at our disposal the central values of the potential parameters and their covariance matrix, we sample, in addition to set S_0 of central values of potential parameters, 50 sets $S_i, i = 1, 2, \dots, 50$ of the potential parameters from the multivariate normal distribution.

- (2) Computing observables for each set of potential parameters

All results in this work have been obtained in momentum space by resorting to standard partial wave decomposition (PWD). We neglect the Coulomb force and the 3N interaction. For each set S_i ($i = 0, 1, \dots, 50$) defining a NN interaction V , we compute the deuteron wave function by solving the Schrödinger equation. Next, for the same V we solve the Lippmann-Schwinger equation, $t = V + V\tilde{G}_0 t$ (\tilde{G}_0 is the free 2N propagator), to obtain the 2N t -matrix, from which 2N scattering observables are obtained. For 3N system we solve the Faddeev equation and construct the transition amplitudes from which the 3N scattering observables are computed, see Chap. IV. For more details on these calculations we refer the reader to Refs. [32, 33] and references therein. As a result, an angular dependence of various np and nd elastic scattering observables is obtained for each set of parameters S_i .

The resulted predictions can be used to study:

- (2,1) for a given observable X at an energy E and at a scattering angle θ , the empirical probability density function of the observable $X(E, \theta)$ resulting when various sets $S_i, (i = 0, \dots, 50)$ are used;
- (2,2) for a given observable X , both the angular and energy dependencies of predictions based on various sets S_i .

This, in turn, allows us to analyze correlations among all observables.

- (2,3) We calculate a sample estimator of the correlation coefficient between two chosen observables X and Y , using the standard formula

$$r(X, Y) = \frac{\sum_{i=1}^n (x_i - \bar{X})(y_i - \bar{Y})}{\sqrt{\sum_{i=1}^n (x_i - \bar{X})^2 \sum_{i=1}^n (y_i - \bar{Y})^2}}, \quad (2.1)$$

where the index “ i ” runs over the sets of $n = 51$ versions of potentials, \bar{X} and \bar{Y} are means: $\bar{X} = \frac{1}{n} \sum_{i=1}^n x_i$ and $\bar{Y} = \frac{1}{n} \sum_{i=1}^n y_i$, respectively.

The interpretation of the correlation coefficient is to some extent arbitrary. The correlation coefficient takes values from -1 to 1 and we define the case $|r| \leq 0.3$ as no correlation,

while $0.3 < |r| \leq 0.5$, $0.5 < |r| \leq 0.7$, and $0.7 < |r| \leq 1$ mean weak, moderate, and strong correlation, respectively. Specifically, $|r(X, Y)| = 1$ means linear dependence between the two observables X and Y . If the correlation coefficient equals 0, then there is no linear dependence between the observables, however, they can still be nonlinearly dependent.

In the determination of the correlation coefficient for a given pair of observables, we have in practice only one 50-element sample at our disposal. Estimation of uncertainty of computed sample correlation coefficients is not straightforward. To find this uncertainty we apply two methods. First we use the well-known Fisher transformation [34, 35]. To construct a confidence interval by Fisher's method, it is assumed that X and Y have a bivariate normal distribution. This assumption is only approximately satisfied by observables, see Ref. [11] for the corresponding discussion on 3N observables obtained with the OPE-Gaussian potential. The variable $Z = \frac{1}{2} \ln \left(\frac{1-r(X, Y)}{1+r(X, Y)} \right)$, which has the standard normal distribution is used to construct a confidence interval at a given confidence level γ . After inverse transformation of the confidence limits one gets the confidence interval for $r(X, Y)$. Applying this method to various pairs (X, Y) , we found that the obtained half confidence interval at $\gamma = 0.9$ is usually ≈ 0.05 for $r \approx 0.9$ and ≈ 0.25 for $r \approx 0.25$.

Secondly, we use the bootstrap resampling method [36–38] to estimate uncertainties of $r(X, Y)$. The advantage of the bootstrap method lies in working directly with sample elements without any assumption about the normality of the X and Y distributions. Resampling (up to 1000 (X, Y) -elements) allows us to find the properties (e.g. distribution or standard derivation) of the bootstrap estimator for the correlation coefficient and thus estimate the uncertainty of originally received $r(X, Y)$, again as a half of bootstrap confidence interval. Typically, the half of the bootstrap confidence interval at $\gamma = 0.9$ is ≈ 0.05 for $r \approx 0.9$ (≈ 0.23 for $r \approx 0.25$). These values are similar to uncertainties resulting from the Fisher method.

This shows that the uncertainty of the correlation coefficients, especially for small $r(X, Y)$, is relatively high. Thus in the following we will restrict ourselves to a more qualitative discussion of correlation coefficients. Since we are interested in finding whether given observables are or are not correlated, such a qualitative result is sufficient.

III. CORRELATIONS AMONG NEUTRON-PROTON ELASTIC SCATTERING OBSERVABLES

Elastic scattering of two spin 1/2 particles offers much more diverse measurements than only of the differential cross section, $d\sigma/d\Omega$, since beside the unpolarized cross section various spin observables are available. In this chapter we present a few observables: the asymmetry A' , the polarization P , the depolarization R , and the spin transfer coefficient D [32]. We determine their correlation coefficients at two incident neutron energies $E_{\text{lab}} = 10$, and 135 MeV in the range of the scattering angle $\theta_{c.m.} \in [12.5^\circ, 167.5^\circ]$ ¹ using the chiral N⁴LO and N⁴LO⁺ SMS NN potentials with the cutoff parameter $\Lambda = 450$ MeV as well as the OPE-Gaussian NN force.

In Fig. 1 we demonstrate, in the form of scatter plots, predictions for the chosen 2N scattering observables based on these three models of the NN potential, using, for each force, 51 sets of potential parameters. The top row in Fig. 1 visualizes a strong positive

¹ This interval was chosen to avoid divergences occurring due to division by a very small value or by zero for $\theta_{c.m.} = 0^\circ$ or $\theta_{c.m.} = 180^\circ$ where the variance of observable tends to zero

correlation between $d\sigma/d\Omega$ and A' at $E_{\text{lab}} = 10$ MeV at three scattering angles $\theta_{c.m.} = 30^\circ$, 90° , and 150° . The correlation coefficients for the chiral N⁴LO SMS force are $r(\theta_{c.m.} = 30^\circ) = 0.81$, $r(\theta_{c.m.} = 90^\circ) = 0.99$, $r(\theta_{c.m.} = 150^\circ) = 0.85$ and $(r(\theta_{c.m.} = 30^\circ) = 0.87$, $r(\theta_{c.m.} = 90^\circ) = 0.99$, $r(\theta_{c.m.} = 150^\circ) = 0.74$ for the OPE-Gaussian potential, so we conclude that the $d\sigma/d\Omega$ and A' are rather strongly correlated at this energy. For $E_{\text{lab}} = 135$ MeV and all three scattering angles, the scatter plots in the second row of Fig. 1, show, that the strong correlation observed at $E_{\text{lab}} = 10$ MeV disappears at higher energy for all the potentials, leaving only weak correlation between ($d\sigma/d\Omega$ and A').

An analysis of two medium rows in Fig. 1 leads to conclusion that $d\sigma/d\Omega$ is weakly correlated with the polarization P , independently of the NN potential used, the scattering energy, and the scattering angle (in fact, that is true for the entire $\theta_{c.m.}$) interval. Yet another pattern of correlations occurs for the (R, A') pair, see two bottom rows of Fig. 1. While at $E_{\text{lab}} = 10$ MeV there is strong positive correlation for all the three scattering angles, at $E_{\text{lab}} = 135$ MeV correlation depends on the scattering angle, changing from strong positive to almost negligible one. Once again we see that the three models of the NN interaction yield similar predictions for the correlation coefficients.

In the case of 2N system we are able to check how our estimation of the correlation coefficients $r(X, Y)$ depends on the sample size and find this dependence very weak. For example a correlation coefficient $r_{50}(X, Y)$ obtained from the 50-element sample calculated with the N⁴LO SMS force and the corresponding correlation coefficient $r_{100}(X, Y)$ derived from the 100-element sample have similar values. In particular, at $E_{\text{lab}} = 10$ MeV and $\theta_{c.m.} = 50^\circ$ the correlation coefficient $r_{50}(d\sigma/d\Omega, R) = 0.95$ while $r_{100}(d\sigma/d\Omega, R) = 0.93$. At $\theta_{c.m.} = 150^\circ$ $r_{50}(d\sigma/d\Omega, R) = 0.82$ and $r_{100}(d\sigma/d\Omega, R) = 0.80$. Similarly, for $r(d\sigma/d\Omega, A')$ we get $r_{50}(d\sigma/d\Omega, A') = 0.88$ and $r_{100}(d\sigma/d\Omega, A') = 0.87$ at $\theta_{c.m.} = 50^\circ$ and $r_{50}(d\sigma/d\Omega, A') = 0.83$ and $r_{100}(d\sigma/d\Omega, A') = 0.78$ at $\theta_{c.m.} = 150^\circ$. At $E_{\text{lab}} = 135$ MeV the correlation coefficients are much smaller: at $\theta_{c.m.} = 50^\circ$ $r_{50}(d\sigma/d\Omega, R) = 0.29$ and $r_{100}(d\sigma/d\Omega, R) = 0.37$, at $\theta_{c.m.} = 150^\circ$ $r_{50}(d\sigma/d\Omega, R) = -0.40$ while $r_{100}(d\sigma/d\Omega, R) = -0.44$. For $r(d\sigma/d\Omega, A')$ we have $r_{50}(d\sigma/d\Omega, A') = 0.24$ and $r_{100}(d\sigma/d\Omega, A') = 0.27$ at $\theta_{c.m.} = 50^\circ$ and $r_{50}(d\sigma/d\Omega, A') = -0.35$ and $r_{100}(d\sigma/d\Omega, A') = -0.41$ at $\theta_{c.m.} = 150^\circ$. While a small (usually about 5%) difference between r_{50} and r_{100} is seen, the qualitative conclusion about correlation coefficients remains unchanged with the increasing sample size. The independence from the sample used is also exemplified in Fig. 2 for $d\sigma/d\Omega$ and A' , where two samples of size 50 yield a similar distribution of predictions.

Focusing on the correlation coefficients we are able now to study their dependence on the scattering angle and the reaction energy in a more compact form than shown in Fig. 1. Figure 3 shows the angular dependence of four correlation coefficients for three energies of the incoming nucleon: $E_{\text{lab}} = 10, 65$, and 135 MeV. Note the range of the Y-axis in Fig. 3 does not cover the full possible range of the correlation coefficient $r \in [-1, 1]$ otherwise many curves would be indistinguishable. The top row, for $r(d\sigma/d\Omega, P)$, shows that at the lowest energy these observables remain uncorrelated for all presented scattering angles, despite differences among predictions based on the considered interactions. At the two higher energies the pattern of angular dependence is more complex and beside ranges of very weak or medium correlation for both chiral models $d\sigma/d\Omega$ and P are strongly correlated around $\theta = 50^\circ$ at $E_{\text{lab}} = 135$ MeV. As seen from the second row of Fig. 3, the np differential cross section $d\sigma/d\Omega$ is, in general, strongly correlated with the asymmetry A' over a wide range of the scattering angle at the incoming neutron laboratory energy $E_{\text{lab}} = 10$ MeV. A magnitude of the $r(d\sigma/d\Omega, A')$ exceeds at this energy 0.8 in a wide range of the scattering angle. For

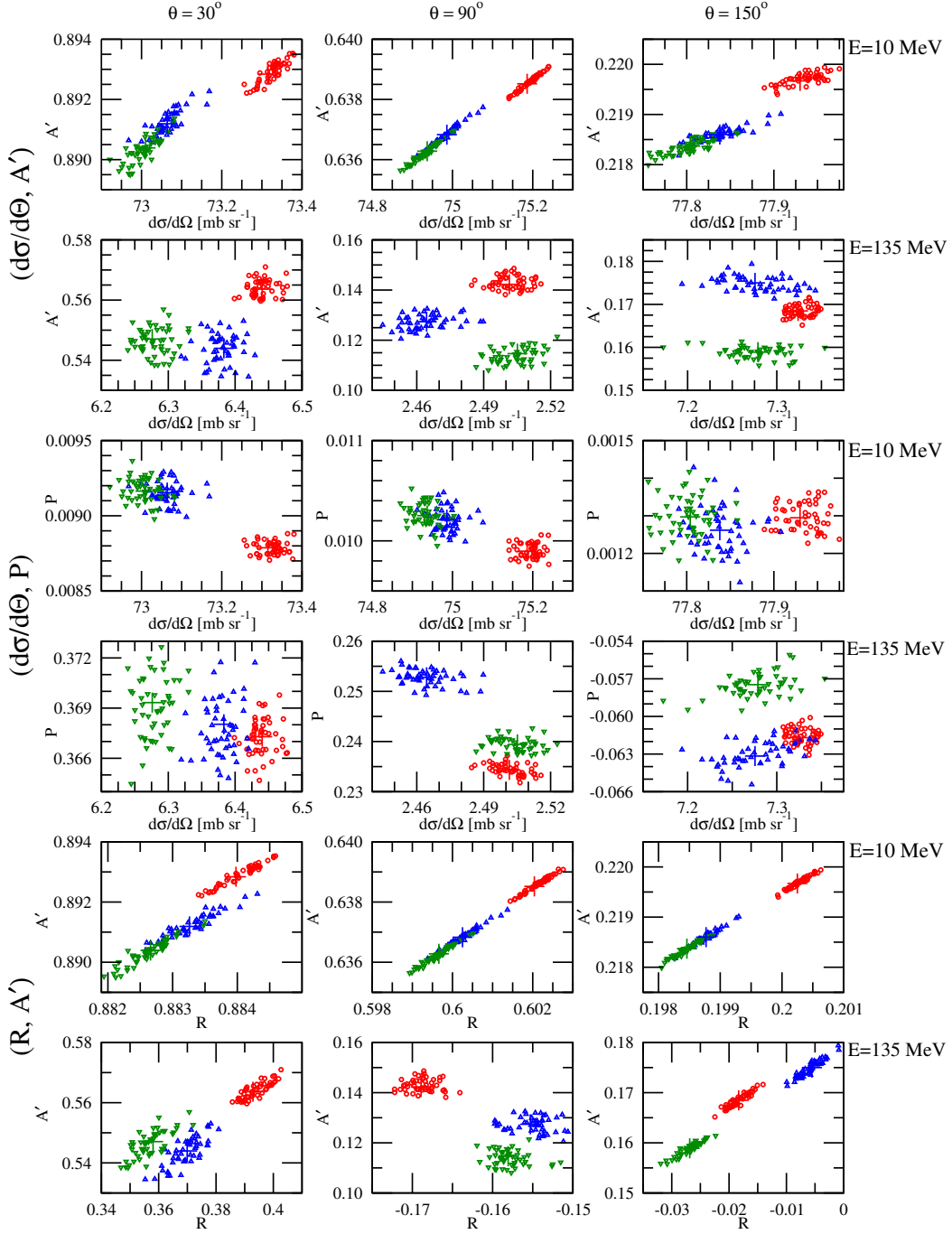


FIG. 1. Scatter plots for the chosen np scattering observables at the c.m. scattering angle $\theta_{c.m.} = 30^\circ$ (left), $\theta_{c.m.} = 90^\circ$ (middle), and $\theta_{c.m.} = 150^\circ$ (right) and at the incoming neutron laboratory energy $E_{\text{lab}} = 10$ MeV (odd rows) and $E_{\text{lab}} = 135$ MeV (even rows). Two top rows are for the differential cross section $d\sigma/d\Omega$ and the asymmetry A' , two middle rows are for the np differential cross section $d\sigma/d\Omega$ and the polarization P and two bottom rows are for the np depolarization R and the asymmetry A' . The blue up-pointing triangles, green down-pointing triangles and red circles show predictions of 50 sets of potential parameters of the chiral $N^4\text{LO}$ ($\Lambda = 450$ MeV), chiral $N^4\text{LO}^+$ ($\Lambda = 450$ MeV) SMS force and the OPE-Gaussian potential, respectively. The single pluses show predictions obtained with the central values of these potentials.

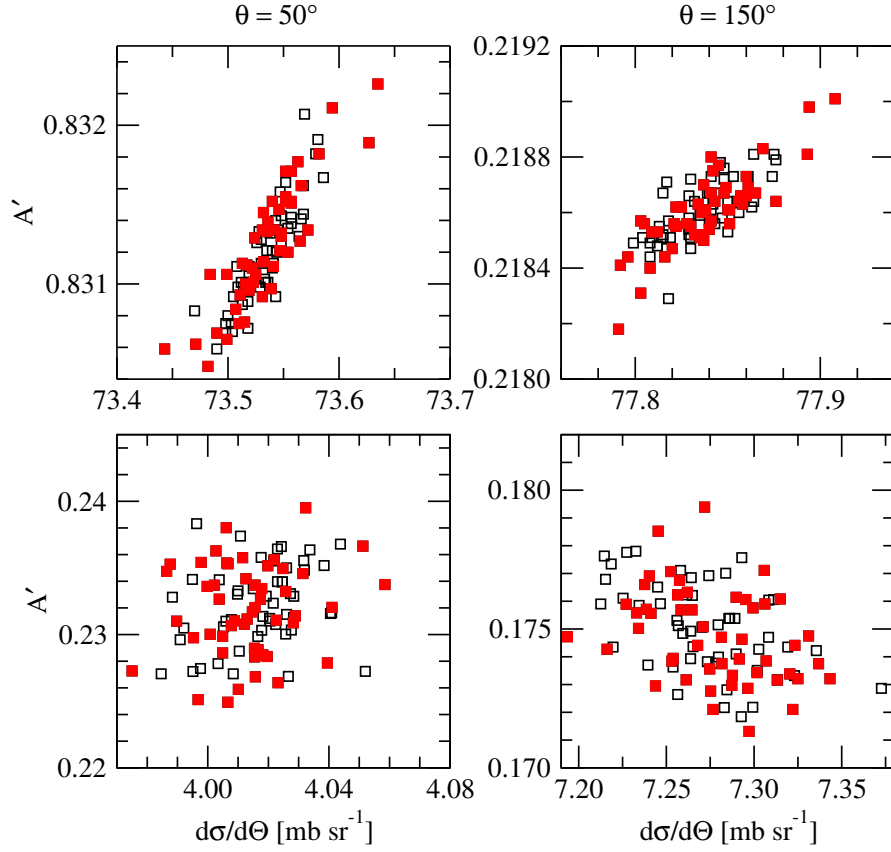


FIG. 2. Scatter plots for $d\sigma/d\Omega$ and A' in np scattering at the c.m. scattering angle $\theta_{c.m.} = 50^\circ$ (left) and $\theta_{c.m.} = 150^\circ$ (right) and at the incoming neutron laboratory energy $E_{\text{lab}} = 10$ MeV (top) and $E_{\text{lab}} = 135$ MeV (bottom) based on two 50-elements sets of potential parameters, represented by the open black squares and the full red squares. The chiral SMS potential at $N^4\text{LO}$ with $\Lambda = 450$ MeV was used.

the two higher energies ($E_{\text{lab}} = 65$ and 135 MeV) the correlation decreases, but still at some regions remains moderate. Figure 3 shows also the angular dependence of the correlation coefficient for the (R, A') pair, which is strongly correlated for all interactions at $E_{\text{lab}} = 10$. At $E_{\text{lab}} = 65$ MeV, the magnitude of the correlation coefficient still has high values, but in the interval $\theta_{c.m.} \in (100^\circ, 150^\circ)$ reaches its minimum of $r \approx 0.65$ for the chiral $N^4\text{LO}$ SMS potential ($r \approx 0.75$ for $N^4\text{LO}^+$). At $E_{\text{lab}} = 135$ MeV, strong correlation is observed at $\theta_{c.m.} \in (50^\circ, 70^\circ)$ and only negative moderate correlation occurs at $\theta_{c.m.} \in (110^\circ, 130^\circ)$. Finally, in the last row of Fig. 3 we display $r(R, D)$, which is close to 1 for the lowest energy, but changes with the increasing energy, ending at $E_{\text{lab}} = 135$ MeV in moderate positive correlation with an exception around $\theta_{c.m.} = 60^\circ$, where a moderate negative correlation is observed.

Combining all the given above observations for the correlation coefficients among 2N observables and not shown here results for other pairs of 2N observables we conclude:

- (1) we observe a complex dependence of the correlation coefficients on the scattering angle and this complexity grows with the reaction energy. While at small energies there are many correlated observables, this picture changes for the higher energies, where more

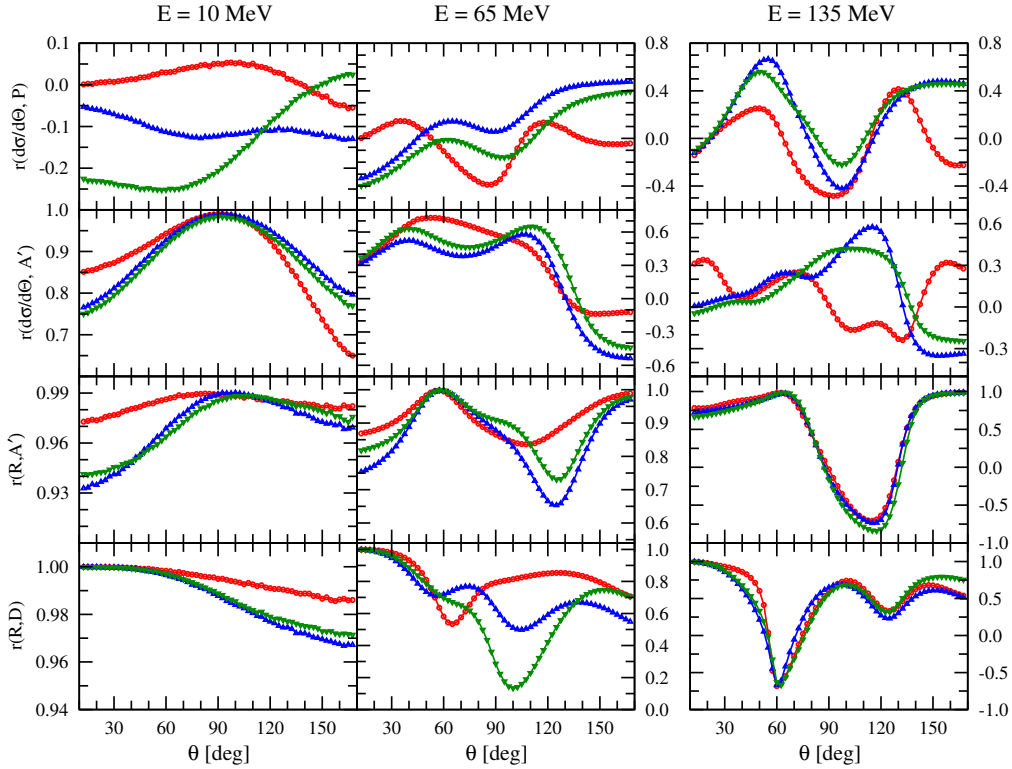


FIG. 3. The angular dependence of correlation coefficients $r(d\sigma/d\Omega, P)$ (top), the $r(d\sigma/d\Omega, A')$ (the second row), $r(R, A')$ (the third row), and $r(R, D)$ (bottom) in np scattering at the incoming neutron laboratory energy $E_{\text{lab}} = 10$ MeV (left), $E_{\text{lab}} = 65$ MeV (middle), and $E_{\text{lab}} = 135$ MeV (right). The red curve with circles, the blue curve with up-pointing triangles, and the green curve with down-pointing triangles represent predictions of the OPE-Gaussian, the SMS $N^4\text{LO}$, and the SMS $N^4\text{LO}^+$ interactions, respectively.

and more observables become uncorrelated. We suppose this effect is related to a bigger number of partial waves (and thus also potential parameters) contributing at higher energies. Due to this complex pattern and relatively big uncertainties of the correlation coefficients, especially for small correlation coefficients, we restrict ourselves to only qualitative conclusions.

- (2) correlation coefficients predicted from various models of the NN interaction, that is from the chiral potentials at various orders and the more phenomenological OPE-Gaussian force, are in qualitative agreement. The observed differences are well inside the uncertainty of the obtained correlation coefficients. Thus, in practice it is possible to conclude about the correlation strength using a sample of parameters from only one model of interaction.
- (3) the polarization P is weakly correlated with the other 2N scattering observables. This is true for all NN potentials (in the case of the chiral SMS forces starting from $N^3\text{LO}$), the scattering energies and scattering angles.
- (4) the differential cross section $d\sigma/d\Omega$ is strongly correlated with all 2N scattering ob-

servables, except for P , at energies up to $E_{\text{lab}} = 30$ MeV, in specific intervals of $\theta_{c.m.}$.

- (5) a sample of 50 sets of potential parameters is sufficient to study correlations between 2N observables. Such a study was impossible with availability of only few models of the NN potential for which only central values of parameters were known.

IV. CORRELATIONS AMONG NEUTRON-DEUTERON ELASTIC SCATTERING OBSERVABLES

We investigate the 3N system within the Faddeev formalism [32, 33, 39]. In the following we will just briefly describe the key equations used in this work.

Since we also studied correlations of scattering observables with the ${}^3\text{H}$ binding energy, beside the scattering states we also computed the ${}^3\text{H}$ bound state for all S_i sets of the potential parameters. The Faddeev-component $|\psi_1\rangle$ of the 3N bound state $|\Psi\rangle$ fulfills [40]

$$|\psi_1\rangle = G_0 t P |\psi_1\rangle, \quad (4.1)$$

where the two-nucleon t -operator, defined in the previous section, acts now in the 3N space. G_0 is the free 3N propagator and P is a permutation operator built from transpositions P_{ij} : $P = P_{12}P_{23} + P_{13}P_{23}$. The complete 3N bound state $|\Psi\rangle = (1 + P)|\psi_1\rangle$.

The transition amplitude U for the Nd elastic scattering is calculated prior to computing 3N scattering observables. Its matrix elements between the initial $|\phi\rangle$ and final $|\phi'\rangle$ Nd states, neglecting 3NF, are given by [33]

$$\langle\phi'|U|\phi\rangle = \langle\phi'|PG_0^{-1}|\phi\rangle + \langle\phi'|PT|\phi\rangle. \quad (4.2)$$

The Faddeev equation for the auxiliary state $T|\phi\rangle$ with nucleons interacting only via a NN interaction V entering a t -matrix expresses as [33]

$$T|\phi\rangle = tP|\phi\rangle + tPG_0T|\phi\rangle. \quad (4.3)$$

In the above equations the initial and final Nd states are products of the deuteron state $|\varphi_d\rangle$ and a relative momentum eigenstate of the free nucleon, $|\vec{q}_0\rangle$, $|\phi\rangle = |\varphi_d m_d\rangle |\vec{q}_0 m_N\rangle$ with the corresponding spin quantum numbers m_d and m_N , respectively.

Applying partial wave decomposition to operators and states in Eqs. (4.1) and (4.3) we solve them numerically, generating for Eq. (4.3) its Neumann series and summing it up using the Padè method [32, 33]. The 3N partial wave basis comprises all states with the two-body subsystem total angular momentum $j \leq 5$ and the total 3N angular momentum $J \leq \frac{25}{2}$. This guarantees convergence of predictions with respect to these total angular momenta. The total number of the 3N states for given J^π (total 3N angular momentum with parity π equal +1 or -1) amounts up to 142. We use grids of 32 p points in the range 0-40 fm^{-1} and 37 q points in the range 0-25 fm^{-1} both for the chiral SMS force and the OPE-Gaussian potential. From Eq. (4.2) one finds matrix elements of the elastic transition amplitude U , from which a large set of observables can be computed [33]. In total, there are 55 different observables for elastic scattering comprising the unpolarized cross section $d\sigma/d\Omega$, nucleon and deuteron analyzing powers, spin correlation coefficients and polarization transfer coefficients from nucleon/deuteron to nucleon/deuteron; for more

details see Ref. [33]. It gives $\frac{1}{2} \times 55 \times 54 = 1485$ pairs of observables, so in the following we choose and describe only a few examples.

We present results for 3N observables in the same way as in the 2N case, i.e. first we discuss scatter plots and next move to the angular dependence of the correlation coefficients.

The scatter plots for the differential cross section $d\sigma/d\Omega$ and the spin correlation coefficient C_{XX} are shown in two upper rows of Fig. 4 for three scattering angles, $\theta_{c.m.} = 30^\circ, 90^\circ$ and 150° , and two laboratory kinetic energies of the incoming nucleon, $E_{lab} = 13$ MeV and $E_{lab} = 135$ MeV. As in the two-body case, we use the chiral N⁴LO and N⁴LO⁺ SMS potentials at $\Lambda = 450$ MeV, and the OPE-Gaussian force. The $d\sigma/d\Omega$ appears strongly correlated with C_{xx} at $\theta_{c.m.} = 90^\circ$ and $\theta_{c.m.} = 150^\circ$ for $E_{lab} = 13$ MeV, and moderately correlated at the three scattering angles at $E_{lab} = 135$ MeV for all the employed potentials. We find that for $\theta_{c.m.} = 30^\circ$ at the lower energy only a weak correlation for this pair of 3N observables exists.

Another picture emerges for the neutron analyzing power $A_y(n)$ and the deuteron vector analyzing power iT_{11} which are strongly or moderately correlated, depending on the scattering angle and energy, see the 3rd and 4th rows of Fig. 4. The N⁴LO (N⁴LO⁺) potential yields for $E_{lab} = 13$ MeV: at $\theta_{c.m.} = 30^\circ$ $r = 0.95$ ($r = 0.94$), at $\theta_{c.m.} = 90^\circ$ $r = 0.90$ ($r = 0.63$), and at $\theta_{c.m.} = 150^\circ$ $r = 0.99$ ($r = 0.99$). For $E_{lab} = 135$ MeV, the dependence between the observables looks very linear at $\theta_{c.m.} = 30^\circ$ and indeed the magnitudes of r are: $\theta_{c.m.} = 30^\circ$ $r = 0.99$ ($r = 0.98$) for the N⁴LO (N⁴LO⁺) forces. The same interactions lead at $\theta_{c.m.} = 90^\circ$ to $r = 0.60$ ($r = 0.33$), and at $\theta_{c.m.} = 150^\circ$ $r = 0.71$ ($r = 0.77$) with N⁴LO (N⁴LO⁺).

Finally, in the two bottom rows of Fig. 4 we demonstrate yet another pattern for the correlation coefficient, which occurs for the spin correlation coefficient C_{XX} and the spin transfer coefficient $K_y^{y'}(n)$. Here, at lower energy and $\theta_{c.m.} = 30^\circ$ and $\theta_{c.m.} = 90^\circ$ the observables are strongly anticorrelated, while at $\theta_{c.m.} = 150^\circ$ we observe strong positive correlation. This picture changes significantly when moving to the higher energy: there is no correlation at $\theta_{c.m.} = 30^\circ$ but a strong positive correlation at $\theta_{c.m.} = 90^\circ$ and $\theta_{c.m.} = 150^\circ$.

Comparison between predictions of the chiral potentials and the OPE-Gaussian model reveals the very similar pattern of correlations. The “cloud” of predictions has usually the same shape for all used forces what leads to comparable values of the correlation coefficient. To give an example: in the case of $(A_y(n), iT_{11})$ pair the OPE-Gaussian potential predicts the correlation coefficients: $r = 0.89$ at $\theta_{c.m.} = 30^\circ$, $r = 0.95$ at $\theta_{c.m.} = 90^\circ$, and $r = 0.98$ at $\theta_{c.m.} = 150^\circ$ for $E_{lab} = 13$ MeV ($r = 0.99$ at $\theta_{c.m.} = 30^\circ$, $r = 0.61$ at $\theta_{c.m.} = 90^\circ$, and $r = 0.45$ at $\theta_{c.m.} = 150^\circ$ for $E_{lab} = 135$ MeV).

From other, not shown here, scatter plots it can be generally concluded that for the vast majority of selected angles at $E_{lab} = 13$ MeV there is often a strong correlation, or less often observed moderate correlation. At the higher energy, $E_{lab} = 135$ MeV, we typically observe a weak correlation at almost all scattering angles, but there are exceptions that indicate a moderate correlation. We can also conclude, that the correlation coefficients for Nd scattering observables predicted with the OPE-Gaussian, N⁴LO, or N⁴LO⁺ forces usually lead to the same qualitative conclusion about the correlation/uncorrelation. The biggest differences in predicted values of the correlation coefficients occur for uncorrelated or weakly correlated cases what is in agreement with our estimation of correlation coefficients uncertainties.

Let us now turn to the angular dependence of the correlation coefficients. We exemplify it in Fig. 5, for the $r(d\sigma/d\Omega, C_{xx})$, $r(A_Y(n), iT_{11})$ and $r(C_{XX}, K_Y^{Y'}(n))$ at three scattering

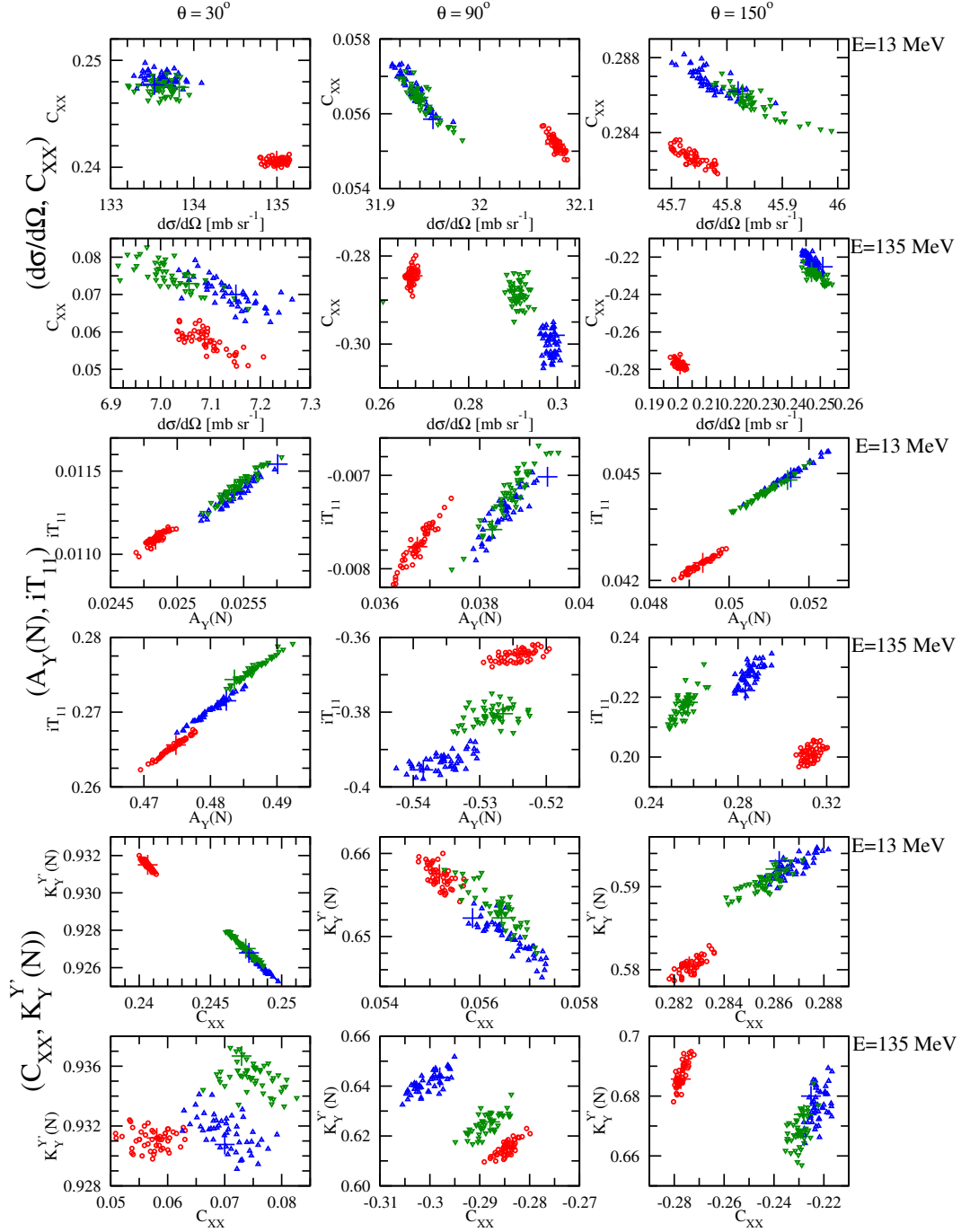


FIG. 4. A scatter plot between $(d\sigma/d\Omega, C_{xx})$, $(A_Y(n), iT_{11})$, and $(C_{xx}, K_Y^y(n))$ in the elastic nd scattering at the c.m. scattering angle $\theta_{c.m.} = 30^\circ$ (left), $\theta_{c.m.} = 90^\circ$ (middle), and $\theta_{c.m.} = 150^\circ$ (right) and at the incoming neutron laboratory energy $E_{lab} = 13$ MeV (odd rows) and $E_{lab} = 135$ MeV (even rows). The red circles, blue up-pointing triangles and the green down-pointing triangles represent results obtained with the OPE-Gaussian force, the N⁴LO SMS and the N⁴LO⁺ SMS potentials, respectively. Pluses in the same colors shows predictions obtained with central values of the parameters.

energies $E_{\text{lab}} = 13, 65$ and 135 MeV. The predicted correlation coefficients are, as in the 2N case, complicated, energy-dependent, functions of the scattering angle so again we restrict ourselves to qualitative conclusions only. The differential cross section $d\sigma/d\Omega$ is, in general, moderately correlated with C_{xx} for the chiral SMS at both presented orders, and for the OPE-Gaussian potential at all energies. However, we can also observe a weak or a strong correlation in some ranges of the scattering angle. A weak correlation for this pair is observed at forward scattering angles at $E_{\text{lab}} = 13$ MeV, for $70^\circ < \theta_{c.m.} < 150^\circ$ at $E_{\text{lab}} = 65$ MeV, and for $45^\circ < \theta_{c.m.} < 140^\circ$ at $E_{\text{lab}} = 135$ MeV. Strong anticorrelation is found at $E_{\text{lab}} = 13$ MeV in the case of $N^4\text{LO}^+$ SMS predictions for $75^\circ < \theta_{c.m.} < 115^\circ$ but with the increasing scattering angle it changes to strong correlation for $120^\circ < \theta_{c.m.} < 140^\circ$. With increasing energy a strong correlation appears at forward/backward scattering angles. It is interesting that at the two lowest energies the $N^4\text{LO}$ SMS and OPE-Gaussian predictions are close one to another while the $N^4\text{LO}^+$ SMS results show a slightly different pattern. However, this is not very important for our qualitative study of the correlation coefficients and does not affect our general conclusion about the weak/moderate dependence between these 3N observables.

The $(A_Y(n), iT_{11})$ pair remains strongly correlated at the two lower energies practically for all the scattering angles. At $E_{\text{lab}} = 135$ MeV the correlation coefficient is close to one only for scattering angles below $\theta_{c.m.} \approx 40^\circ$ and correlation becomes moderate for bigger angles. Again at lower energies $N^4\text{LO}^+$ predictions are slightly different from the $N^4\text{LO}$ and OPE-Gaussian ones.

Yet another pattern emerges for $r(C_{XX}, K_Y^{Y'}(n))$ and is displayed in the bottom row of Fig. 5. Here at the highest energy all predictions are close one to another and reveal weak, moderate or even strong correlation, depending on the range of the scattering angle. At two lower energies all predictions, in general, also show a similar behaviour; however at $E_{\text{lab}} = 13$ MeV the $N^4\text{LO}^+$ results show much stronger minimum around $\theta_{c.m.} = 135^\circ$ than the two remaining predictions.

Conclusions arising from this analysis of Fig. 5 (and not shown here results for other pairs of 3N observables) are as follows:

- (1) the angular dependence of the correlation coefficients reveals complex structures for all pairs of observables and energies. These structures are a consequence of nonlinear dependence of the observables on potential parameters. In addition, the fact that the genuine potential parameters are fitted after the partial wave decomposition of the NN potential makes this relation even more hidden. Also our method of calculating r , which is based on a sample of 50 predictions, introduces additional uncertainty. Nevertheless, tests performed in the 2N system, and the fact that using different potentials (therefore different parameter spaces) leads to similar conclusions about the strength of correlations, seem to prove the correctness of the picture obtained.
- (2) in most cases, the $N^4\text{LO}$ and $N^4\text{LO}^+$ yields similar correlation coefficients, although there are also pairs of 3N observables for which they significantly differ for $120^\circ < \theta_{c.m.} < 150^\circ$, especially at $E_{\text{lab}} = 13$ MeV. Beside $(C_{xx}, K_y^{y'}(n))$ considered in Fig. 5 these are: $(C_{zz}, K_z^{z'}(d))$, $(K_y^{y'}(n), K_x^{x'}(n))$, $(K_y^{y'}(n), K_y^{y'}(d))$, $(K_y^{y'}(n), K_z^{z'}(d))$, $(K_y^{y'}(n), K_x^{x'}(d))$, and $(K_y^{y'}(n), K_z^{z'}(d))$.
- (3) at $E_{\text{lab}} = 13$ MeV 3N observables are usually strongly correlated for $\theta_{c.m.} < 120^\circ$ when the chiral $N^4\text{LO}^+$ SMS potential is used. They become moderately or weakly

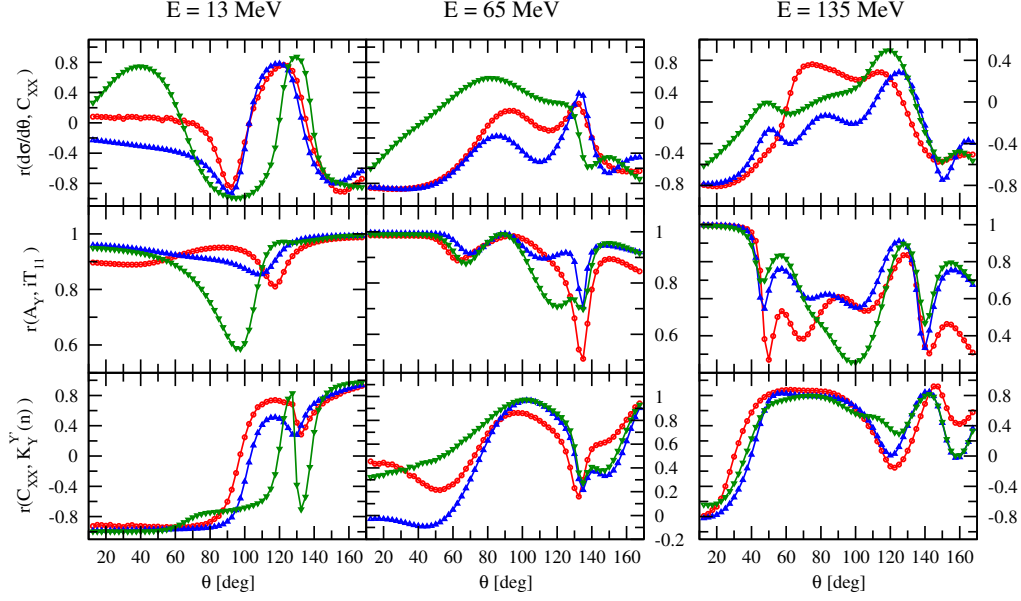


FIG. 5. The angular dependence of correlation coefficients r between $d\sigma/d\Omega$ and C_{XX} (top), the $A_Y(n)$ and iT_{11} (the second row), and the C_{XX} and $K_Y^{y'}(n)$ (bottom) in the nd scattering at the incoming neutron laboratory energy $E_{\text{lab}} = 13$ MeV (left), $E_{\text{lab}} = 65$ MeV (centre), and $E_{\text{lab}} = 135$ MeV (right). The red curve with circles, the blue curve with up-pointing triangles, and the green curve with down-pointing triangles represent predictions of the OPE-Gaussian, the SMS $N^4\text{LO}$, and the SMS $N^4\text{LO}^+$ interactions, respectively.

correlated or even uncorrelated above this angle up to $\theta_{c.m.} \approx 150^\circ$ where again strong correlation is seen.

- (4) among the most easily experimentally available observables, i.e. the differential cross section, the neutron vector analyzing power $A_Y(n)$, the deuteron vector analyzing power iT_{11} and the deuteron tensor analyzing powers T_{20} , T_{21} and T_{22} , only the $(A_Y(n), iT_{11})$ pair shows strong correlation in the whole range of the scattering angle. The (T_{20}, T_{21}) and (T_{20}, T_{22}) are strongly correlated for scattering angles $\theta_{c.m.}$ below below approx. 80° at the lowest studied energy $E_{\text{lab}} = 13$ MeV. At higher energies, all these observables, with the exception of $(A_Y(n), iT_{11})$ are characterized by weak correlation for a wide range of the scattering angle with correlation coefficients in the range of $-0.5 < r < 0.5$.
- (5) in the case of the $N^2\text{LO}$ SMS force at all considered energies the correlation coefficient undergoes stronger changes with the scattering angle than the correlation coefficients computed with other potentials. The observed stabilization at higher orders shows that restricting calculations to the third order of the chiral expansion can be misleading for some correlation coefficients at the energies studied here.
- (6) the absolute value of the correlation coefficient decreases with increasing energy, which indicates weak correlation or even no correlation, with rare exceptions of $(C_{xx}, K_y^{y'}(n))$ (Fig. 5) and $(C_{zz}, K_y^{y'}(d))$ pairs. For other observables at $E_{\text{lab}} = 65$ and 135 MeV strong/moderate correlation appears only in specific intervals of the scattering angles.

This is true for all the used NN forces: the chiral SMS N⁴LO, N⁴LO⁺, and the OPE-Gaussian potentials.

All the SMS chiral force based results presented above have been obtained with the regularization parameter $\Lambda = 450$ MeV. It is also interesting to study the sensitivity of correlation coefficients to the value of that cutoff parameter. Figure 6 demonstrates this dependence at N⁴LO⁺ using three values of Λ : 450, 500, and 550 MeV for the pairs (C_{xx}, C_{yy}) (the top row) and $(A_y(n), iT_{11})$ (the bottom row). What is interesting - the cutoff dependence of $r(C_{xx}, C_{yy})$ is the most significant at the lowest energy $E_{\text{lab}} = 13$ MeV, while at the two higher energies predictions are close to each other, leading firmly to the same quantitative conclusion on correlation between these observables. In contrast, at $E_{\text{lab}} = 13$ MeV and $\theta_{c.m.} \approx 90^\circ$ for $\Lambda = 500$ and 550 MeV we obtain a weak or moderate correlation, while for $\Lambda = 450$ the correlation remains strong. Also at $\theta_{c.m.} \approx 135^\circ$ the predictions based on $\Lambda = 450$ cutoff yield moderate correlation, while the two other cutoff values suggest strong correlation. Similar picture arises for $r(A_y(n), iT_{11})$ where at the two higher energies, despite some differences between predictions, a qualitative description of correlations is cutoff independent. At $E_{\text{lab}} = 13$ MeV the SMS predictions with $\Lambda = 450$ MeV reveals moderate correlation in comparison to strong correlation resulting when $\Lambda = 500$ MeV or $\Lambda = 550$ MeV is used. At $E_{\text{lab}} = 13$ MeV and for $\Lambda = 550$ MeV there is strong correlation in the whole range of $\theta_{c.m.}$ with the correlation coefficient dropping only to ≈ 0.9 for $\theta_{c.m.} = 112.5^\circ$. The same is observed for $\Lambda = 500$ MeV but r reaches a minimum of ≈ 0.83 for $\theta_{c.m.} = 115^\circ$. At $E_{\text{lab}} = 13$ MeV the cutoff $\Lambda = 450$ MeV provides a gradual decreasing of r from 0.95 at $\theta_{c.m.} = 12.5^\circ$ to $r \approx 0.58$ at $\theta_{c.m.} = 97.5^\circ$, but starting from $\theta_{c.m.} \approx 100^\circ$ $r(A_y(n), iT_{11})$ increases.

Another interesting case of correlation between observables is given by the so-called Phillips line [41], [42] describing a dependence between the ³H binding energy and the nucleon-deuteron doublet scattering length, ²a_{nd}. The Phillips line was observed in the past both in calculations with and without 3NF. As seen from Fig. 7 we reproduce the Phillips line using chiral N³LO, N⁴LO and N⁴LO⁺ SMS interactions with $\Lambda = 450$ MeV. The correlation coefficient between these observables takes values of 0.75, 0.71 (0.97 after removing three outliers), 0.98, and 0.96 for predictions at N²LO, N³LO, N⁴LO, and N⁴LO⁺, respectively. With the increasing chiral order, the values of these two observables change a little but are far from the experimental data ($E(^3H) = -8.4820 \pm 0.0001$ MeV [43] and ²a_{nd} = 0.65 ± 0.04 fm [44]). The observed discrepancy between our present predictions and the data is not surprising as it is well-known that both ³H binding energy and ²a_{nd} are strongly influenced by 3NF.

As mentioned in the introduction, the differential cross section at medium energy and the ³H binding energy $E(^3H)$ are nowadays used to fix parameters of the 3NF in the chiral SMS model. Now we are able to check if these two observables are uncorrelated. This is done in Fig. 8. Indeed, the presented scatter plots confirm no correlation between these two observables. The correlation coefficient $r(d\sigma/d\Omega, E(^3H))$ is small at both energies and for all the scattering angles. Its absolute value remains below $|r| = 0.28$. For not shown here energy 65 MeV $|r(d\sigma/d\Omega, E(^3H))|$ does not exceed $|r| \approx 0.3$. We expect that this picture will not change for complete predictions comprising 3NF.

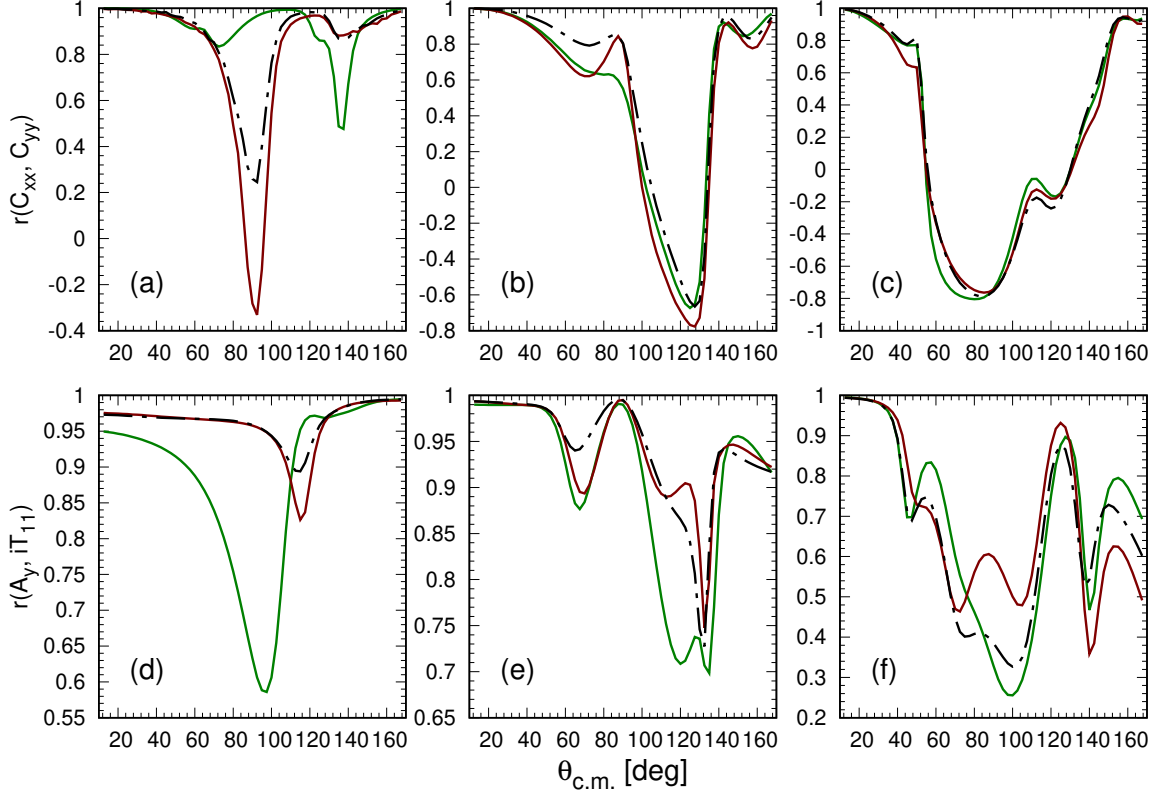


FIG. 6. The angular dependence of correlation coefficients $r(C_{xx}, C_{yy})$ (top) and $r(A_y(n), iT_{11})$ (bottom) for different cutoff values (450 MeV — green solid curve, 500 MeV — maroon solid curve, and 550 MeV — black dot-dashed curve) for the SMS force at $N^4\text{LO}^+$ order and at the incoming neutron laboratory energies $E_{\text{lab}} = 13$ MeV (left), $E_{\text{lab}} = 65$ MeV (center) and $E_{\text{lab}} = 135$ MeV (right).

V. SUMMARY AND OUTLOOK

In the presented work we give a systematic analysis of the correlation coefficients among 2N and 3N observables. We demonstrated that it is possible to analyze correlations among various 2N and 3N observables using the covariance matrices of potential parameters provided with the models of NN interactions from the Granada and Bochum-Bonn groups. Consequently, we showed that there are pairs of 2N spin observables for which an almost linear dependence exists, as documented by correlation coefficients close to ± 1 . For example, these are the cases of the np depolarization R and the asymmetry A' or of the differential cross section and the asymmetry A' . Correlations between given observables are observed both for the chiral SMS force (at $N^3\text{LO}$ and beyond) and for the OPE-Gaussian potential. For some pairs of 2N observables, the angular dependence of the correlation coefficients depends strongly on the order of the chiral expansion as well as on the scattering energy.

The same is true for elastic neutron-deuteron scattering. All correlation coefficients change in a complicated way with the scattering angle. For many pairs of 3N observables we found intervals of scattering angles where the correlation coefficient $|r| > 0.8$. We also studied the dependence of the correlation coefficients on the order of the chiral expansion and on the scattering energy. For some pairs of the spin correlation and spin transfer co-

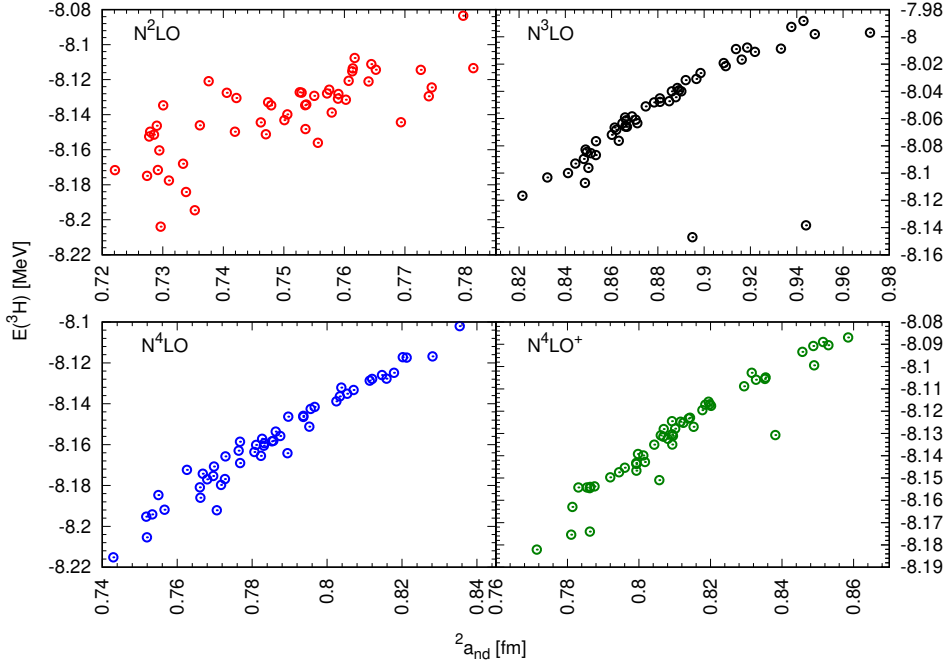


FIG. 7. Order-by-order results ($N^2\text{LO}$ – $N^4\text{LO}^+$ with $\Lambda = 450$ MeV) for the Phillips line $E(^3\text{H})$ – $^2a_{\text{nd}}$.

efficients, as well as for the analyzing powers, a moderate dependence on the chiral cutoff parameter Λ is observed. However, in most cases it does not change our qualitative conclusions on the correlation/uncorrelation between specific observables. Our results reflect a complex dependence of observables on potential parameters. Our calculations reproduce the Phillips line $E(^3\text{H})$ – $^2a_{\text{nd}}$ and support the practice of determining values of free parameters of the three-nucleon interaction from the uncorrelated differential cross section and the triton binding energy.

The next step in studies of correlations in few-nucleon systems is to investigate the sensitivity of a given observable to the value of a specific potential parameter. In such a case one deals with nonlinear dependence of observables on many, mutually correlated, potential parameters. Thus much more sophisticated statistical tools than the sample correlation coefficient must be applied. Information about sensitivity of some 2N or 3N observables to a given potential parameter can be used to improve a procedure of fixing potential parameters. Existence of strongly correlated observable-potential parameter pairs could also motivate experimental groups to perform precise measurements of such observable, especially if the experimental data are not yet available.

ACKNOWLEDGMENTS

We would like to thank Dr E.Epelbaum and Dr P.Reinert from the Ruhr-Universität, Bochum, for providing us with the potential chiral subroutines. This work was partly supported by the National Science Centre of Poland under grant number UMO-2020/37/B/ST2/01043 and by PL-GRID infrastructure. The numerical calculations were partly performed on the

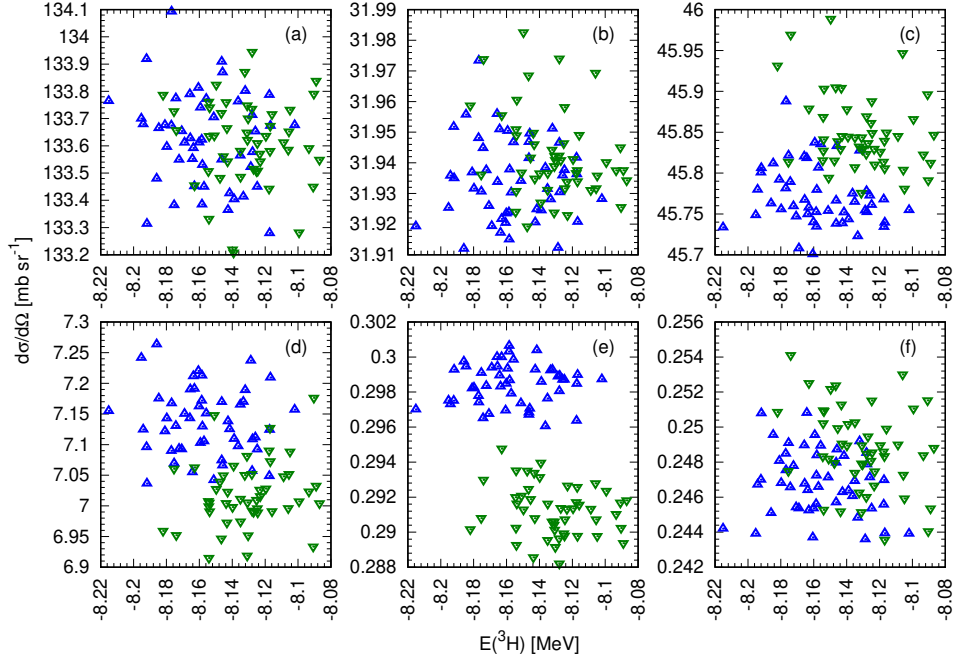


FIG. 8. A scatter plot between the nd elastic differential cross section $d\sigma/d\Omega$ and the triton binding energy $E(^3H)$ at the c.m. scattering angle $\theta_{c.m.} = 30^\circ$ (left), $\theta_{c.m.} = 90^\circ$ (middle), and $\theta_{c.m.} = 150^\circ$ (right) and at the incoming neutron laboratory energy $E_{lab} = 13$ MeV (top) and $E_{lab} = 135$ MeV (bottom). The blue up-pointing triangles (the green down-pointing triangles) represent the chiral NN SMS predictions at N^4LO (N^4LO^+).

supercomputer cluster of the JSC, Jülich, Germany.

-
- [1] R. B. Wiringa, V. G. J. Stoks, and R. Schiavilla, *Phys. Rev. C* **51**, 38 (1995).
 - [2] R. Machleidt, *Phys. Rev. C* **63**, 024001 (2001).
 - [3] V. G. J. Stoks, R. A. M. Klomp, M. C. M. Rentmeester, and J. J. de Swart, *Phys. Rev. C* **48**, 792 (1993).
 - [4] E. Epelbaum and U.-G. Meißner, *Annual Review of Nuclear and Particle Science* **62**, 159 (2012), <https://doi.org/10.1146/annurev-nucl-102010-130056>.
 - [5] P. Reinert, H. Krebs, and E. Epelbaum, *Eur. Phys. J. A* **54**, 86 (2018).
 - [6] D. R. Entem, R. Machleidt, and Y. Nosyk, *Phys. Rev. C* **96**, 024004 (2017).
 - [7] M. Piarulli, L. Girlanda, R. Schiavilla, A. Kievsky, A. Lovato, L. E. Marcucci, S. C. Pieper, M. Viviani, and R. B. Wiringa, *Phys. Rev. C* **94**, 054007 (2016).
 - [8] L. E. Marcucci ed., *Frontiers in Physics Special Issue: The Long-Lasting Quest for Nuclear Interactions: The Past, the Present and the Future* (Lausanne, Frontiers Media SA, 2021).
 - [9] R. N. Pérez, J. E. Amaro, and E. R. Arriola, *Phys. Rev. C* **88**, 064002 (2013).
 - [10] R. N. Pérez, J. E. Amaro, and E. Ruiz Arriola, *Phys. Rev. C* **89**, 064006 (2014).
 - [11] R. Skibiński, Y. Volkotrub, J. Golak, K. Topolnicki, and H. Witała, *Phys. Rev. C* **98**, 014001 (2018).

- [12] Y. Volkotrub, J. Golak, R. Skibiński, K. Topolnicki, H. Witała, E. Epelbaum, H. Krebs, and P. Reinert, *Journal of Physics G: Nuclear and Particle Physics* **47**, 104001 (2020).
- [13] S. Coon, M. Scadron, P. McNamee, B. Barrett, D. Blatt, and B. McKellar, *Nuclear Physics A* **317**, 242 (1979).
- [14] S. A. Coon and W. Glöckle, *Phys. Rev. C* **23**, 1790 (1981).
- [15] S. Coon and H. Han, *Few-Body Systems* **30**, 131 (2001).
- [16] B. S. Pudliner, V. R. Pandharipande, J. Carlson, S. C. Pieper, and R. B. Wiringa, *Phys. Rev. C* **56**, 1720 (1997).
- [17] E. Epelbaum, A. Nogga, W. Glöckle, H. Kamada, U.-G. Meißner, and H. Witała, *Phys. Rev. C* **66**, 064001 (2002).
- [18] E. Epelbaum, W. Glöckle, and U.-G. Meißner, *Nuclear Physics A* **747**, 362 (2005).
- [19] R. Skibiński, J. Golak, K. Topolnicki, H. Witała, E. Epelbaum, W. Glöckle, H. Krebs, A. Nogga, and H. Kamada, *Phys. Rev. C* **84**, 054005 (2011).
- [20] A. Phillips, *Nuclear Physics A* **107**, 209 (1968).
- [21] P. Maris, E. Epelbaum, R. J. Furnstahl, J. Golak, K. Hebeler, T. Hüther, H. Kamada, H. Krebs, U.-G. Meißner, J. A. Melendez, A. Nogga, P. Reinert, R. Roth, R. Skibiński, V. Soloviov, K. Topolnicki, J. P. Vary, Y. Volkotrub, H. Witała, and T. Wolfgruber (LENPIC Collaboration), *Phys. Rev. C* **103**, 054001 (2021).
- [22] K. Sekiguchi, H. Sakai, H. Witała, W. Glöckle, J. Golak, M. Hatano, H. Kamada, H. Kato, Y. Maeda, J. Nishikawa, A. Nogga, T. Ohnishi, H. Okamura, N. Sakamoto, S. Sakoda, Y. Satou, K. Suda, A. Tamii, T. Uesaka, T. Wakasa, and K. Yako, *Phys. Rev. C* **65**, 034003 (2002).
- [23] E. Epelbaum, J. Golak, K. Hebeler, T. Hüther, H. Kamada, H. Krebs, P. Maris, U.-G. Meißner, A. Nogga, R. Roth, R. Skibiński, K. Topolnicki, J. P. Vary, K. Vobig, and H. Witała (LENPIC Collaboration), *Phys. Rev. C* **99**, 024313 (2019).
- [24] L. Girlanda, A. Kievsky, L. E. Marcucci, and M. Viviani, *Phys. Rev. C* **102**, 064003 (2020).
- [25] H. Witała, J. Golak, and R. Skibiński, *Eur. Phys. J. A* **57**, 1 (2021).
- [26] H. Witała, J. Golak, and R. Skibiński, arXiv preprint (2022), 10.48550/arXiv.2203.08499.
- [27] R. N. Pérez, A. Nogga, J. E. Amaro, and E. R. Arriola, *Journal of Physics: Conference Series* **742**, 012001 (2016).
- [28] J. Kirscher, H. W. Griebhammer, D. Shukla, and H. M. Hofmann, *EPJ Web of Conferences* **3**, 04005 (2010).
- [29] A. Kievsky, M. Viviani, D. Logoteta, I. Bombaci, and L. Girlanda, *Phys. Rev. Lett.* **121**, 072701 (2018).
- [30] J. Tjon, *Physics Letters B* **56**, 217 (1975).
- [31] A. G. Escalante, R. N. Pérez, and E. R. Arriola, *Phys. Rev. C* **104**, 054002 (2021).
- [32] W. Glöckle, *The quantum mechanical few-body problem*, Texts and monographs in physics (Springer, Berlin, 1983).
- [33] W. Glöckle, H. Witała, D. Hüber, H. Kamada, and J. Golak, *Physics Reports* **274**, 107 (1996).
- [34] R. Fisher, *Biometrika* **10**, 507 (1915).
- [35] R. Fisher, *Metron* **1**, 1 (1921).
- [36] B. Efron, “Bootstrap methods: Another look at the jackknife,” in *Breakthroughs in Statistics: Methodology and Distribution*, edited by S. Kotz and N. L. Johnson (Springer New York, New York, NY, 1992) pp. 569–593.

- [37] O. Ikpotokin and I. Edokpa, *International Journal of Scientific & Engineering Research* **4**, 1695 (2013).
- [38] A. Bishara and J. Hittner, *Behavior research methods* **49**, 294 (2017).
- [39] H. Witała, W. Glöckle, J. Golak, A. Nogga, H. Kamada, R. Skibiński, and J. Kuroś-Żołnierczuk, *Phys. Rev. C* **63**, 024007 (2001).
- [40] A. Nogga, D. Hüber, H. Kamada, and W. Glöckle, *Physics Letters B* **409**, 19 (1997).
- [41] A. Phillips, *Nuclear Physics A* **107**, 209 (1968).
- [42] V. Efimov and E. Tkachenko, *Physics Letters B* **157**, 108 (1985).
- [43] R. N. Pérez, E. Garrido, J. E. Amaro, and E. Ruiz Arriola, *Phys. Rev. C* **90**, 047001 (2014).
- [44] W. Dilg, L. Koester, and W. Nistler, *Physics Letters B* **36**, 208 (1971).